MyoPassivity Map: Does Multi-Channel sEMG Correlate With the Energetic Behavior of Upper-Limb Biomechanics During Physical Human-Robot Interaction?

Suzanne Oliver , *Graduate Student Member, IEEE*, Peter Paik , *Graduate Student Member, IEEE*, Xingyuan Zhou , *Graduate Student Member, IEEE*, and S. Farokh Atashzar , *Senior Member, IEEE*

Abstract—The human arm has an intrinsic capacity to absorb energy during physical human-robot interaction (pHRI), which can be identified as biomechanical excess of passivity (EoP). This can be used as a central factor in the development of passivity-based pHRI controllers securing haptic transparency while guaranteeing pHRI stability. Despite its significance, the real-time estimation of EoP remains an under-investigated topic. For the first time, we investigate the relationship between the EoP and muscle activity of the forearm at the wrist joint while analyzing sixteen surface electromyography (sEMG) sensors. The letter explores optimal sensor placement for maximizing the correlation between muscle activity and the estimated EoP. Ten subjects participated in this study. The EoP of the wrist was identified through high-frequency perturbations in four directions, and two instructed co-contraction levels. The results uncover a strong correlation between sEMG and EoP. This paper also reports the effect of the direction of pHRI interaction on the EoP of the wrist, with increased energetic passivity in the abduction-adduction direction compared to supination-pronation. Also, the study investigated the effect of the observation duration for sEMG on the sEMG-EoP correlation (short windows would be required for real-time applications). Although the correlation decreases for shorter windows, it remains relatively high, supporting dynamic estimation of EoP in real-time. Additionally, we found that sEMG sensors near the wrist have the highest correlation with EoP for short windows. The findings of this letter indicate that sEMG encodes significant potential for real-time estimation of EoP in the design of next-generation pHRI controllers supporting concurrent transparency and stability.

I. INTRODUCTION

THE characteristics of physical human-robot interaction (pHRI) are a fundamental aspect of several human-centered robotic systems, such as telerobotics, an exponentially growing field due to the evolution of next-generation communication, extended reality, and AI. With a variety of applications, including rehabilitation, surgery, and robot-mediated remote human-human interaction, this technology is stepping us towards a smarter and more connected society [1], [2], [3]. Haptics-enabled pHRI embedded in such systems would ideally provide a natural and intuitive bidirectional interface for the users allowing for an immersive experience [4] and enhancing the capabilities of such robotic systems in various fields. For example, in the area of medical robotics, haptics-enabled pHRI and tele-pHRI can augment the targeted performance in surgery or can allow for a wide range of rehabilitative tasks in robotic telerehabilitation platforms [5], [6], [7]. For designing any haptics-enabled pHRI, there are two main challenges that should be considered and addressed, namely: 1) guaranteeing the overall safety of the physical interaction between human biomechanics and powered robot mechanics, 2) maximizing the fidelity of the energy exchange and rendered haptics interaction. The aforementioned two design criteria have been shown to be opposing, meaning that a perfectly transparent system is at the edge of instability, which can sacrifice safety [8], [9], [10].

In addition to classic issues, such as internal sensor noise or actuator failure [11], stability can be further hindered when controlling a pHRI over a network due to non-ideal quality of service of communication channels, such as delay, jitter, and packet loss [12], [13], [14], [15]. Mathematically, it can be shown that the aforementioned issues result in the injection of non-passive energy into the interconnected systems, putting stability, and thus safety, at more significant risk. In addition, in some specialized tasks, such as assistive robots that inject energy for empowering disabled users, a high assistive loop gain [16] will be another source of non-passive energy injection in the system, which further increases the risk of exacerbating system

Suzanne Oliver is with the Department of Mechanical and Aerospace Engineering, New York University (NYU), New York, NY 11201 USA (e-mail: sho8511@nyu.edu).

Peter Paik and Xingyuan Zhou are with the Department of Electrical and Computer Engineering, New York University (NYU), New York, NY 11201 USA (e-mail: hsp287@nyu.edu; xz3428@nyu.edu).

S. Farokh Atashzar is with the Departments of Electrical and Computer Engineering, Mechanical and Aerospace Engineering, and Biomedical Engineering, New York University (NYU), New York, NY 11201 USA, and also with the NYU WIRELESS Center and NYU CUSP, Brooklyn, NY 11201 USA (e-mail: f.atashzar@nyu.edu).

instability and limits the functionality of classic passivity-based stabilizers that assume a dissipative dynamical behavior for the rendered haptics field [8], [9], [10], [13], [14]. As a result, various research teams have investigated solutions to the instability issue in recent years while focusing on reducing the conservatism of the proposed algorithms (some examples are as follows: [8], [17], [18], [19], [20], [21], [22], [23], [24], [25], [26], [27]). Many of the recent solutions are rooted in the formulation of the Time Domain Passivity Approach (TDPA) [23], which is widely used for ensuring the stability of classic teleoperation systems.

TDPA ensures stability by observing the energy flow of a closed-loop system and dispersing the extra energy as needed by injecting damping (altering the communicated force and velocity). However, due to the fact that TDPA and other passivity-based controllers unavoidably modify the delivered force and/or velocity, a degradation of the system's transparency/performance occurs at the expense of stability. This can be problematic in advanced technologies such as rehabilitation robotics and exoskeletons, which require the robot to impart large forces on the user to assist them in completing the tasks [8], [28]. Degradation of the transmitted force/velocity can lead to degradation of perceptual causality and quality of information exchange, and potential failures of the task.

There are some recent works that have investigated the impedance of the human limb as a novel modality for interaction in telerobotic systems based on the concept of teleimpedance [20], [21], [27], [29]. This approach can allow for controlling a teleoperated robot in a way that follows the impedance-based commands from the human when closing the loop. In this letter, instead of teleoperatively rendering the impedance of humans, we look into the nonlinear capacity of the arm in absorbing the energy from the telerobotic system, a biomechanical passivity index that can be exploited to enhance the transparency and increase the stability margin. It should also be highlighted that a limitation of classic TDPA is the exclusion of the impact of the "passivity index" of human biomechanics in the pHRI loop. Atashzar et al. have shown that even utilizing a fixed and minimum lower bound of the human biomechanical energy absorption capacity significantly enhances the performance of the controller and improves functionality and transparency [9], [10], [14].

In order to incorporate the energy absorption capacity of human biomechanics into the closed loop of haptics systems, the intrinsic and inherent biomechanical passivity margin of the user should be quantified in real-time, for which more sensory information is needed besides force and motion sensors; otherwise, the mathematical problem will be ill-conditioned [9], [30]. For this, we have recently proposed the use of the concept of "Excess of Passivity" (EoP) from nonlinear control theory in the context of pHRI, which can be used as an indicator of the nonlinear energetic behavior of the human limbs [8], [9], [10], [14], [30]. Previous attempts to quantify the EoP of the human upper limb utilize offline calculations to create a map of the user's EoP when moving in different directions with a range of strength of grip, all of which factor into the passivity and vary depending on the user's biomechanics [9]. However, the feasibility of real-time estimation of EoP has not been investigated in the past. Access to information regarding the underlying neurophysiology can help to predict the corresponding changes in the biomechanics during various muscle contractions and thus changes in EoP.

This work is the first attempt towards investigating if and how the activation of forearm muscles correlates to the energy absorption capability of the upper arm. In this letter, we focus on the wrist joint, which is the most critical due to its direct physical engagement with the robotic handle. As the biosignal modality, we used surface Electromyography (sEMG) to detect the propagation and distribution of the underlying muscle activities and map this information into the EoP of the arm. Additionally, we compared sixteen locations for sEMG sensors on the forearm to determine the optimal location for a sensor to maximally correlate with the EoP and with the changes of the EoP in real-time.

A robust experimental setup was formulated to test and measure the EoP while measuring sixteen sEMG channels, placed on the Brachioradialis, Flexor Carpi Radialis, Extensor Carpi Ulnaris and Extensor Digitorum muscles [31]. The experiment was run on ten subjects by perturbing their wrists in four directions: abduction, adduction, pronation, and supination. For this work, the perturbation frequencies were set in the typical frequency range of voluntary human interaction as suggested in the literature [10], [32]. We found that at both the group level and individual level, the correlation between muscle activation and EoP is significantly strong and is highest for sensors closer to the hand.

Since the proposed method is user-specific, it can be tailored for users for use in rehabilitation robotics as long as there is enough residual sEMG and muscle power for the patient to be eligible for the use of typical rehabilitation robotic systems. It should be noted that sEMG has been used to drive rehabilitation robots in the literature, which demonstrates the feasibility of this approach for rehabilitation patients [33].

In this letter, we also investigated the effect of the window of observation aiming for real-time applications. The results would allow the generation of future stabilizers that can dynamically track the energetic capacity of human biomechanics and use that to minimize the conservatism of control structure, maximizing agility and haptic transparency while preserving the stability of pHRI systems, which is imperative for medical applications.

II. METHODS

A. Excess of Passivity of Human Biomechanics

Atashzar et al. have formulated the mathematical base to show that the passivity of an interconnected system (e.g., a negative interconnection between humans and (tele)robots) can be written as the interplay between the excess of passivity of human biomechanics and summations of all non-passive energy such as those generated by the non-passive communication network and those by non-passive haptics force rendering in assistive systems (details can be found in [9], [10], [14], [30]). In this regard, the following definition would be needed to explain the energetic capacity of human biomechanics.

Definition 1 (Output Strictly Passive System): An Output Strictly Passive (OSP) system with input variable $U(t)$, output variable $Y(t)$, and initial energy $E(T_s)$ is defined as:

$$\int_{T_s}^{T_e} U(t)^T Y(t) dt + E(T_s) \geq \xi \int_{T_s}^{T_s} Y(t)^T Y(t) dt, \quad (1)$$

with a non-negative EoP coefficient of ξ. T_s represents the start time and T_e represents the end time of the perturbation window. The OSP system is L2 stable with a finite L2 gain of $1/\xi$ [34]. Meanwhile, according to the (1), if $\xi < 0$, the system is regarded

TABLE I
DEMOGRAPHIC DATA

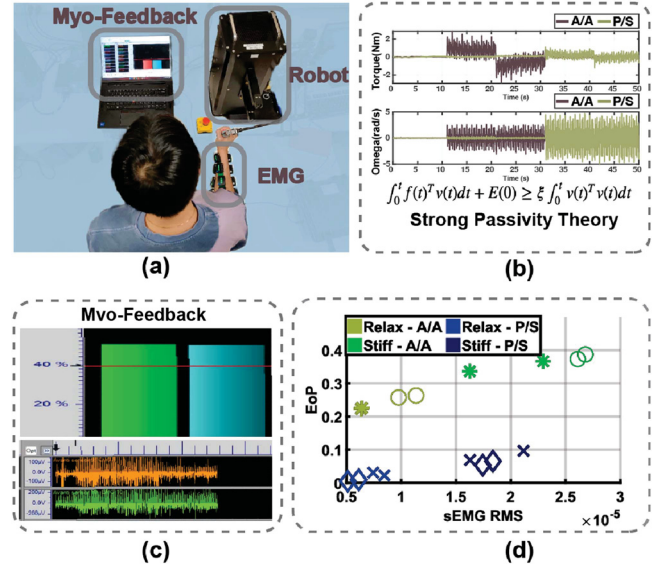| Subject	Height (m)	Weight (kg)	Age	Sex
1	1.62	58	24	M
2	1.77	64	25	M
3	1.70	59	25	F
4	1.87	77	32	M
5	1.70	59	25	F
6	1.72	58	33	F
7	1.75	75	25	M
8	1.76	60	26	M
9	1.55	63	20	F
10	1.63	75	22	F

Fig. 1. (a) Experimental setup. (b) Example of torque and angular velocity profiles. (c) Visual of EMG myofeedback in real-time. (d) Resulting relationship between EMG and EoP.

to be Output Non-Passive (ONP) with a Shortage of Passivity (SoP) coefficient of ξ.

Using the OSP definition and relaxing the classic assumption of linearity on human biomechanics, an estimate of the excess of passivity of human biomechanics can be calculated as follows during an identification process. In this regard, τ is the applied perturbation torque to the wrist, and ω is the resulting measured angular velocity of the wrist during identification.

$$\xi = \frac{\int_{T_s}^{T_e} \tau(t)^T \omega(t) dt}{\int_{T_s}^{T_e} \omega(t)^T \omega(t) dt} \qquad (2)$$

In the context of pHRI, a higher value of EoP corresponds to a higher absorption capacity of interactive energy. This value uncovers an inherent passivity margin which can be exploited by any passivity stabilizers.

B. Experiment Design and Procedure

Ten healthy subjects (five males and five females, mean age 25.7 ± 4.0 years) participated in this experiment. The study was approved by the Institutional Review Board of New York University. Each subject signed a written consent form prior to beginning the experiment. All subjects denied a history of musculoskeletal injury or impairment. Demographic information of the subjects is shown in Table I.

An identification experiment was designed to investigate the relationship between the recorded 16-channel sEMG and EoP for each individual. The setup for this experiment is shown in Fig. 1. For the EoP identification, a Quansar High Definition Haptic Device (Quansar, Markham ON, Canada) robot was used to perturb the subject's wrist in four directions, i.e., abduction, adduction, pronation, and supination. The perturbation signal was a mixed-frequency sinusoidal wave, ranging from 1 Hz to 5 Hz. The angle of oscillation was between $0°$ to $30°$ centered at $15°$ for each direction for ten seconds.

Each subject completed (a) two trials with a relaxed co-contraction and (b) two trials with a high co-contraction (defined by a stiff grip) using visual myofeedback, as explained below. The order of the trials was randomized for each subject. Due to the high artifact at the moment of transition from one direction
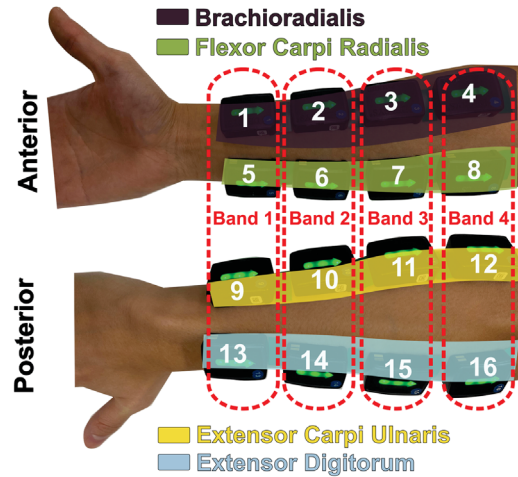

Fig. 2. Placement of sEMG sensors along forearm muscles.

to another, the first five seconds of data in each direction was discarded.

Sixteen wireless Bipolar Delsys Trignosystem (Delsys, Natick, MA, USA) EMG sensors were placed on the forearm of the subject, along the Brachioradialis, Flexor Carpi Radialis, Extensor Carpi Ulnaris, and Extensor Digitorum muscles. The sensors recorded at a sampling rate of 1778 Hertz. The layout of the sEMGs is shown in Fig. 2. Before beginning the trials, the maximum voluntary contraction (MVC) of the participant was recorded for Sensors 2 and 11 to be used for visual feedback during the experiment.

For the above-mentioned myofeedback, during the identification experiments, users were visually provided with a real-time measurement of their co-contraction level from Sensors 2 and 11, during each trial, in the form of percent MVC. An example is shown in Fig. 1(c). For the stiff contraction, subjects were asked to grasp the robotic handle while maintaining 40% MVC. For the relaxed state, subjects were asked to maintain below 5% of their MVC (a light contact between the robot handle and their
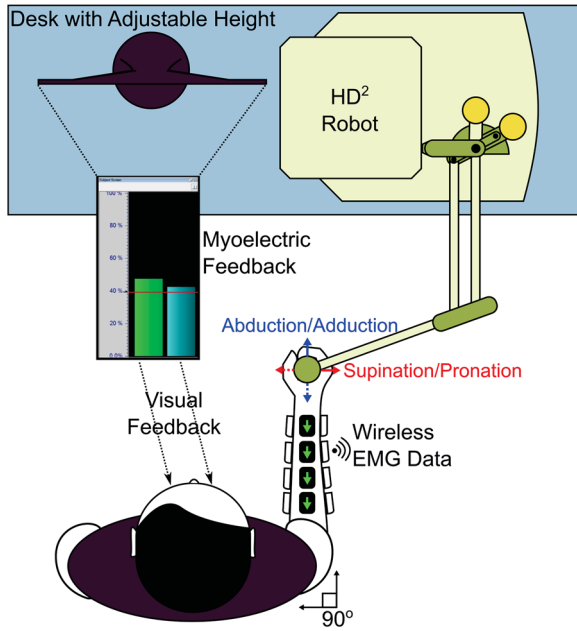
Fig. 3. Experimental setup showing the posture of the subject, high definition haptic robot, myoelectric bar feedback, and Delsys wireless system.

fingers and palm). During the experiment, subjects were asked to stand with their upper arm against their torso and elbow at a $90°$ angle, with their forearm extending directly ahead. The wrist was initially in a neutral position, with the fingers wrapped around the vertical handle of the robot before the perturbations began. The robot was placed on a height-adjustable table to allow for consistent posture between subjects of varying heights. The myofeedback display was placed directly in front of the user, so they could see it without disturbing their posture. The subjects were not harnessed to avoid disrupting their natural biomechanics and to mimic the expected conditions (reactive biomechanics) during a pHRI task. It should be noted that there is the possibility of energy coupling between the joints in the experimental scenario, which is similar to a typical pHRI. This letter does not isolate the energetic behavior of each joint from the rest of the biomechanics. The setup is designed to closely resemble a practical pHRI scenario without adding extra constraints. The experimental setup is provided in Fig. 3.

C. Data Analysis

The data from the sEMG sensors and the robot was processed in MATLAB. The EoP was calculated as described in Section II-A. The sEMG signals were filtered with a bandpass filter between 20 and 500 Hz and bandstop filters of width 4 Hz at multiples of 60 Hz (for power-line noise). The filters were 4th order Butterworth filters. The data was then epoched into segments of equal length for further processing. To investigate the effect of window size, we considered segment lengths of 5 seconds, 0.1 seconds, and 0.01 seconds.

From each segment, the Root-Mean-Square (RMS) of the filtered sEMG signal was calculated as $\sqrt{\frac{1}{N}\sum_{i=1}^{N} X_i^2}$, where N is the number of points in the segment and X_i is the ith point. This calculation gives us a measure of the signal magnitude. The correlation between the RMS value of sEMG and the mean EoP of the corresponding segment was assessed by the line of best

fit and computing the R^2 value of the fit. Two additional linear regressions were computed for each subject and window size, one using all sixteen sEMG sensors as input and one using the subset of the four sensors closest to the wrist (Sensors 1, 5, 9, and 13) as input. For each regression, the R^2 value between the EoP estimated by the model and the true EoP was calculated.

In order to assess the performance of the sensors relative to each other, the R^2 correlation values were compared, and the statistical significance of the differences was evaluated. Before conducting a significance test, we first performed a Kolmogorov-Smirnov normality test on the distribution of the differences in correlation values for each pair of sensors. The test rejected the null hypothesis of normality at a significance level of 0.05. After the normality test, a right-tailed Wilcoxon signed-rank test was performed on each pair of sensors to determine if there was a significant *increase* in the correlation of one sensor compared to another, again with a significance level of 0.05.

Finally, to evaluate the effect of sensor placement on the R^2 values, the sensors were grouped into four Bands based on distance from the wrist, as shown in Fig. 2. The Kolmogorov-Smirnov normality test also rejected the normality of these distributions, so a two-tailed Wilcoxon signed-rank test was performed to assess the significance of differences in the distributions. Both tests used a significance level of 0.05.

III. RESULTS

Fig. 4 shows the correlation between the sEMG RMS of Sensor 10 (as an example) and the EoP for each subject. The X-axis shows the two tested contraction levels picked up by sEMG, and the Y-axis shows the EoP. The directions of perturbation, i.e., abduction, adduction, pronation, and supination, are shown by various symbols. As expected, there are variations between subjects in the slope of the line of best fit, attributed to biomechanical differences in their arms. It can also be seen that there is a distinct difference between the EoP behavior during perturbations in the pronation/supination orientation (P/S) compared to the abduction/adduction orientation (A/A). The EoP in the A/A direction is higher than in the P/S direction. This trend is consistent among all of the ten subjects. A possible explanation for this phenomenon is that the wrist is less compliant when twisting in the A/A direction.

Going beyond the result for only one sensor, Figs. 5 and 6 show the correlations between the EoP and each sEMG sensor and the combined model with all sensors for the P/S and A/A directions separately. The box plots report the corresponding R^2 value of the linear fit for all subjects.

As mentioned before, in this letter, we also investigate the effect of the window of observation on the understudied correlation. From a practical point of view, shorter windows are preferable due to their agility in detecting dynamic changes in the EoP and their real-time implementation. In Figs. 5 and 6, each row corresponds to a different window length (the top row is for 5-second observation, the middle row is for 100-ms observation, and the bottom row is for 10-ms observation). As can be seen in the aforementioned figures, using the 5-second window, for all subjects and each sensor, there is a very strong correlation between the EoP and EMG RMS, with a median R^2 score of 0.95 in the P/S case and 0.89 in the A/A case. The results of this letter showed strong performance of the proposed model for the tested levels of co-contraction (the two sides of the co-contraction spectrum: relax and stiff, to cover the range).
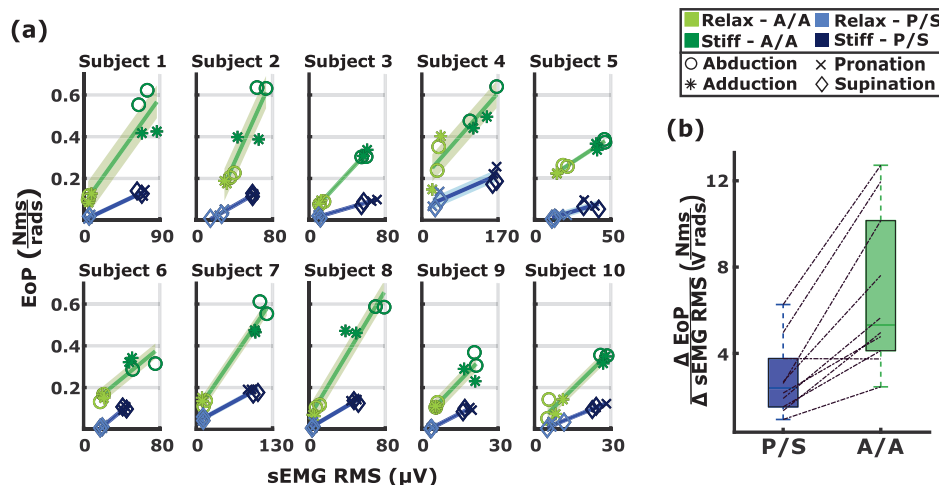
Fig. 4.   (a) Trend between the EoP and sEMG RMS of Sensor 10 for each subject. Separate linear trend lines are shown for the Adduction/Abduction (A/A) and Pronation/Supintation (P/S) correlations. Shaded regions indicate the standard deviation. (b) Box plot distributions of P/S and A/A trend line slopes for all subjects for Sensor 10. Dotted lines indicate the change in slope for each subject.
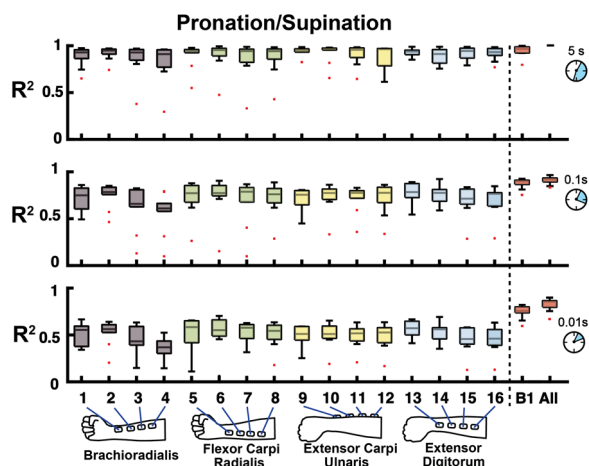

Fig. 5. R^2 values for the trend between EoP and EMG RMS during perturbations in the Pronation/Supination direction for each sensor and for the fit using multiple sensors (labelled 'All' for the model with all sixteen sensors and 'B1' for the model with the four sensors in Band 1), at different epoch lengths (Top: 5 seconds, Middle: 0.1 seconds, Bottom: 0.01 seconds).

Fig. 6. R^2 values for the trend between EoP and EMG RMS during perturbations in the Abduction/Adduction direction for each sensor and for the fit using multiple sensors (labelled 'All' for the model with all sixteen sensors and 'B1' for the model with the four sensors in Band 1), at different epoch lengths (Top: 5 seconds, Middle: 0.1 seconds, Bottom: 0.01 seconds).
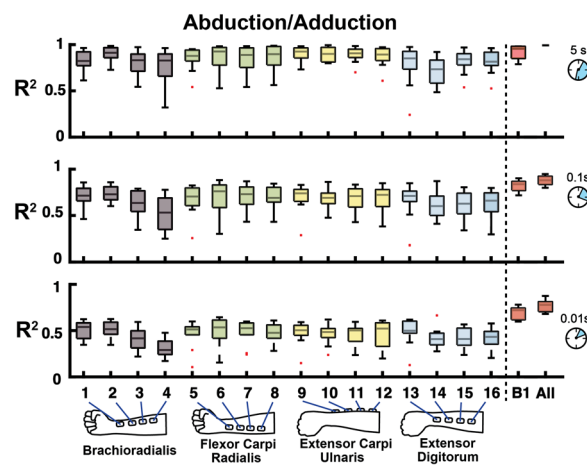
However, it should be noted that the study if limited by the use of only two co-contraction levels. More intermediate ranges of co-contraction will be studied in future work. The results of the statistical test (i.e., right-tailed paired Wilcoxon signed rank test evaluating the significant *increase*) are explained in detail later in this section; however, for the case of 5-second observation for P/S perturbations, it can be mentioned that in almost all cases of comparison, no statistical significance was observed (details below). This suggests that for the 5-second recording window, the EoP v.s. sEMG RMS trend is robust to the sensor location for perturbations in the P/S direction.

However, as mentioned before, in order to use these results in a real-time application and to secure agility in response to dynamic changes in EoP, a smaller window of observation would be desired for updating the EoP estimate. Thus, we investigated the possibility of using shorter windows while maintaining a high level of correlation. The corresponding results can be found

in the second and the third row of Figs. 5 and 6, in which the EoP-sEMG correlation was evaluated for 100-ms and 10-ms observation over all sEMG sensors. As can be seen, the R^2 values between EoP and sEMG RMS decrease as the window shortens, but the correlation does remain relatively high even with short windows securing a median R^2 value of 0.77 in the P/S direction and 0.68 in the A/A direction for a 100-ms recording. As the window gets shorter, we also see more variation between the sensors.

As expected, by significantly increasing the number of sensors in the model to four and then to sixteen, the regression performance increases, and this increase was also modulated by the duration of the window (the higher the window of observation, the better the regression performance). Thus, the combined model using all sensors represents a 'best-case scenario' for EoP approximation using sEMG RMS. For both the 100-ms and 10-ms case, the four-sensor model has a higher correlation

with the true EoP than any individual sensor, and the correlations for the sixteen-sensor model are even higher, with median R^2 values of 0.90 (P/S) and 0.85 (A/A) for the four-sensor model and 0.93 (P/S) and 0.89 (A/A) for the sixteen-sensor model using the 100-ms window. However, it should be added that from a practical point of view, it is strongly desirable to use a lower number of channels and shorter windows (to enable real-time estimation rather than a delayed response). Thus, we next considered the performance differences between the individual sensors to determine the optimal placement for a single sensor.

Fig. 7 shows the difference in median values of correlation (R^2) for each pair of sensors for P/S twists and indicates which sensors have statistically significant increases in the R^2 distributions compared to each other sensor, using a right-tailed Wilcoxon signed-rank test. Since we investigating the optimal sensor placement, we are specifically interested in which sensors outperformed others, instead of simply which sensors had differences in performance. Thus, the right-tailed test was chosen over the two-tailed test. However, it should be noted that the standard for significance is lower for the right-tailed test than a two-tailed test [35]. We see that in the 5-second case, only seven sensor pairs have a statistically significant increase. More specifically, Sensor 10 shows a higher statistical correlation than Sensors 5, 6, 7, and 11; Sensor 9 shows a higher correlation than Sensor 14; and Sensors 3 and 16 have a higher correlation than Sensor 4.

In contrast with the previous case, in the 100-ms and 10-ms cases, there are many significant differences in the P/S direction, and a trend emerges, as explained in the following. For the 100-ms window, Sensors 3 and 4 have significantly lower correlation values than most other sensors. Moving to the 10-ms case, Sensors 3, 4, 15, and 16 have lower correlations than most other sensors. In particular, Sensor 4's correlation is significantly lower than every other sensor for the 10-ms window. It is notable here that all four of these sensors are placed close to the elbow on the *Brachioradialis* (Sensors 3 and 4) and *Extensor Digitorum* (Sensors 15 and 16) muscles (we call these four the elbow-group sensor set).

These results suggest that increased distance from the wrist along the *Brachioradialis* and *Extensor Digitorum* muscles decreases the correlation between EoP and sEMG for P/S perturbations for the short time windows. To support this finding, Fig. 9 shows the distributions of R^2 values for each sensor and subject using the 10-ms window, grouped by the sensor distance from the wrist. The sensors placed closest to the wrist (Band 1) have significantly higher R^2 values than those further from the wrist (Bands 3 and 4).

In contrast, Sensors 6, 10, 11, 12, and 13 each significantly outperform the aforementioned elbow group sensors. Three of these five high-performing sensors are placed along the *Extensor Carpi Ulnaris* muscle (i.e., Sensors 10, 11, and 12), which suggests the activation of this muscle has a particularly strong correlation to the EoP.

It should be noted that the magnitude of the differences in the shorter time windows cases are much greater than in the 5-second case, with the maximum difference in median R^2 increasing from 0.05 to 0.18 and 0.22, for the 100-ms and 10-ms windows, respectively. Correspondingly, the standard deviation of the median R^2 values from each sensor increases from 0.016 for the 5-second case to 0.050 for the 100-ms case and 0.060 for the 10-ms case. This indicates a greater variability between
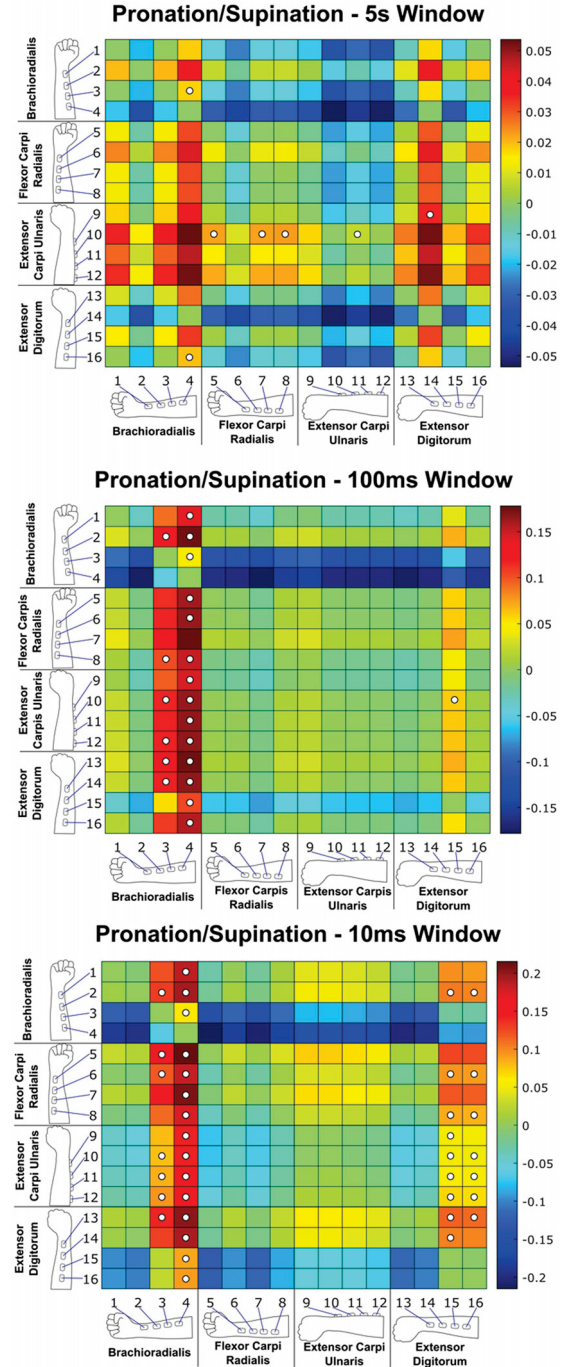

Fig. 7. Pronation/Supination heatmaps showing the difference between medians (over subjects) of R^2 values of sensor pairs (in particular, entry (i, j) represents the median of R^2 value for the ith sensor minus the median of R^2 value for the jth sensor). White dots indicate a statistically significant increase ($p < 0.05$) between the two paired sensor R^2 distributions. Top (5-second window), middle (100-millisecond window), and bottom (10-millisecond window).

sensors using the short time window compared to the longer one for perturbations in the P/S direction.

For the A/A direction, shown in Fig. 8, there are more significant differences in the 5-second case than we saw in the P/S direction, and the magnitude of the difference between median R^2 values is also larger. In this case, Sensor 14 performs the worst and has a significantly lower correlation than twelve of
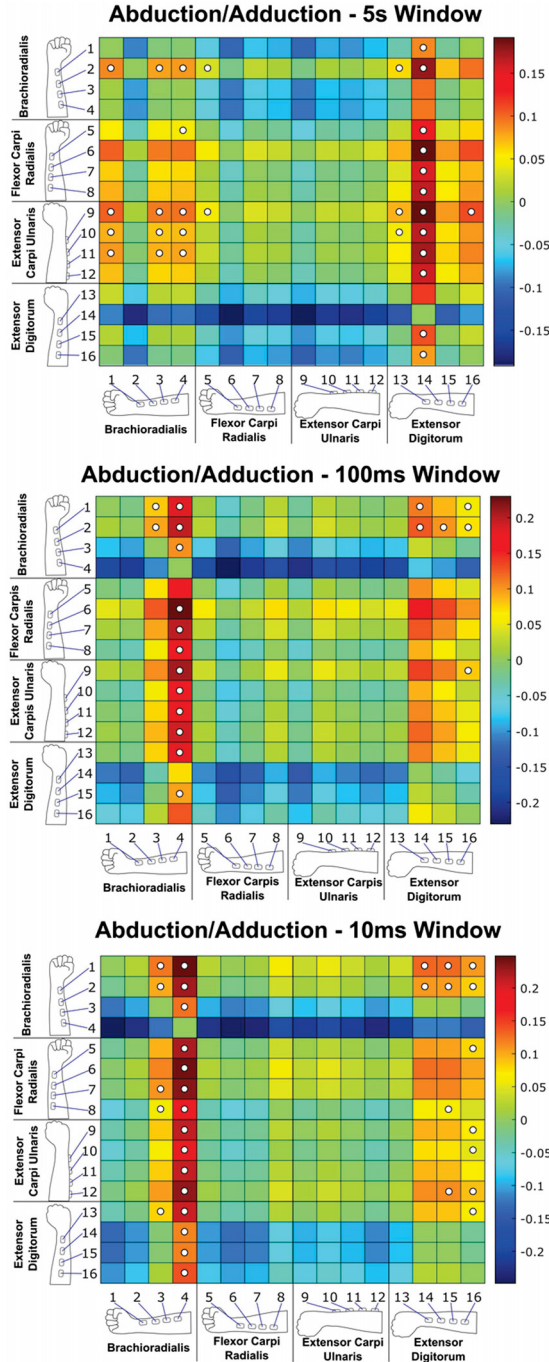
Fig. 8. Abduction/Adduction heatmaps showing the difference between medians (over subjects) of R^2 values of sensor pairs (in particular, entry (i, j) represents the median of R^2 value for the ith sensor minus the median of R^2 value for the jth sensor). White dots indicate a statistical significant increase ($p < 0.05$) between the two paired sensor R^2 distributions. Top (5-second window), middle (100-millisecond window), and bottom (10-millisecond window).

the other sensors. The best-performing sensors are Sensors 9, 10, and 11 (again along the *Extensor Carpi* Ulnaris), as well as Sensor 2 (on the *Brachioradialis*).

It is important to note that for the 100-ms and 10-ms windows of the A/A perturbations, we see a similar trend as in the P/S perturbations. For the 100-ms window, Sensors 3 and 4 again have significantly lower R^2 distributions than most other sensors. In the 10-ms case, the same elbow-group sensor set (i.e.,
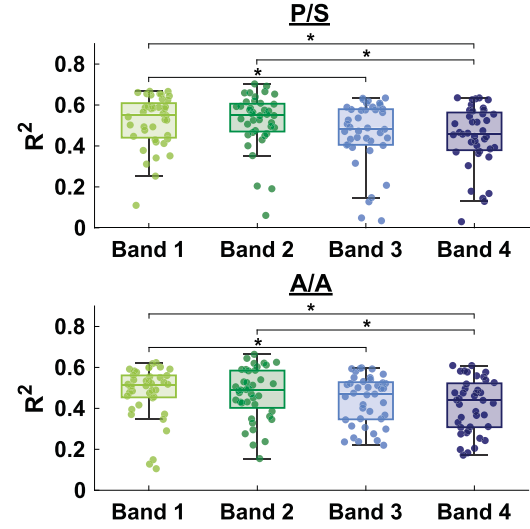

Fig. 9. Distributions of R^2 values for all subjects based on the distance of the sensor from the wrist using the 10-ms window size. Band 1 consists of the four sensors closest to the wrist (Sensors 1, 5, 9, and 13), while Band 4 contains the results from the four sensors furthest form the wrist (Sensors 4, 8, 12, and 16). Results from the P/S (top) and A/A (bottom) perturbations are shown separately. Each dot shows the R^2 value for an individual subject and sensor.

Sensors 3, 4, 15, and 16) we saw in the P/S case have the lowest performance. As before, in the 10-ms case, Sensor 4 has a significantly lower correlation than every other sensor. Additionally, the sensors with the highest correlation, in this case, are Sensors 1 and 2 (close to the wrist on the *Brachioradialis*), indicating that distance from the wrist along this muscle is important for EoP estimating in the A/A direction. As in the P/S case, in Fig. 9, there is a significant difference in the distributions close to the wrist compared to those far from the wrist, further supporting the conclusion that sensor distance from the wrist is important in the 10-ms case.

Also in keeping with the results from the P/S case, the standard deviation of the median R^2 distribution for A/A is larger for the short time windows than in the 5-second case, increasing from 0.051 to 0.060 and 0.066 for 100-ms and 10-ms cases, respectively, indicating there is more variability between sensors using the shorter time window.

IV. CONCLUSION

In this letter, we investigated the relationship between EoP and sEMG for the human upper limb in the frequency range of voluntary human interaction. The ultimate goal of this work is the real-time estimation of excess of passivity (which identifies the energetic behavior of the system, here human biomechanics) to be used in pHRI controllers, enhancing haptic rendering transparency and stability. Ten subjects participated in an experiment to measure muscle activation using multi-channel sEMG sensors while a robot perturbed their wrist, evaluating the energetic behavior of their biomechanics based on the definition of EoP. We found a strong linear correlation between EoP and sEMG for a 5-second window of sEMG observation. For shorter windows, the correlation decreased but still remained relatively strong. We found that for the 5-second window length, the sixteen studied sEMG sensors had a similarly strong correlation for the P/S direction (with a relatively small difference between the median R^2 values across subjects). For the A/A direction

and the 5-second window length, the sensors along *Extensor Carpi Ulnaris* were the most correlated with EoP. For the shorter period (i.e., 100 ms and 10 ms), there was increased variability between sensors for both perturbation directions. We found that sensors placed further from the wrist along the *Brachioradialis* and *Extensor Digitorum* were less correlated with the EoP than sensors close to the wrist and along the other muscles.

The results of this study can be used in the design of haptic systems, rehabilitation robots, surgical robots (with appropriate adaptation due to the delicate nature of surgery), and other areas of pHRI that require high levels of energy exchange between human biomechanics and powered robot mechanics. Because this method is specific to the user, it can be tailored for patients with atrophied muscles due to stroke or other neurological damage for use in rehabilitation robotics. The focus of this work was in the typical frequency range of voluntary human interaction. A separate frequency analysis can be conducted as a future work in this line of research to further shed light on higher frequencies than the typical voluntary range. Future work will also include integrating these findings into a new family of controllers for pHRI.

REFERENCES

[1] L. Onnasch and E. Roesler, "A taxonomy to structure and analyze human–robot interaction," *Int. J. Social Robot.*, vol. 13, no. 4, pp. 833–849, 2021.

[2] A. Mohebbi, "Human-robot interaction in rehabilitation and assistance: A review," *Curr. Robot. Rep.*, vol. 1, pp. 131–144, 2020.

[3] S. Avgousti et al., "Medical telerobotic systems: Current status and future trends," *Biomed. Eng. Online*, vol. 15, no. 1, pp. 1–44, 2016.

[4] V. Villani et al., "Survey on human–robot collaboration in industrial settings: Safety, intuitive interfaces and applications," *Mechatronics*, vol. 55, pp. 248–266, 2018.

[5] K. Veluvolu and W. Ang, "Estimation and filtering of physiological tremor for real-time compensation in surgical robotics applications," *Int. J. Med. Robot. Comput. Assist. Surg.*, vol. 6, no. 3, pp. 334–342, 2010.

[6] R. K. Orosco et al., "Compensatory motion scaling for time-delayed robotic surgery," *Surg. Endoscopy*, vol. 35, pp. 2613–2618, 2021.

[7] M. Shahbazi, S. F. Atashzar, M. Tavakoli, and R. V. Patel, "Robotics-assisted mirror rehabilitation therapy: A therapist-in-the-loop assist-as-needed architecture," *IEEE/ASME Trans. Mechatron.*, vol. 21, no. 4, pp. 1954–1965, Aug. 2016.

[8] S. F. Atashzar, I. G. Polushin, and R. V. Patel, "A small-gain approach for nonpassive bilateral telerobotic rehabilitation: Stability analysis and controller synthesis," *IEEE Trans. Robot.*, vol. 33, no. 1, pp. 49–66, Feb. 2017.

[9] S. F. Atashzar et al., "A grasp-based passivity signature for haptics-enabled human-robot interaction: Application to design of a new safety mechanism for robotic rehabilitation," *Int. J. Robot. Res.*, vol. 36, no. 5/7, pp. 778–799, 2017.

[10] S. F. Atashzar, M. Shahbazi, M. Tavakoli, and R. V. Patel, "A passivity-based approach for stable patient– robot interaction in haptics-enabled rehabilitation systems: Modulated time-domain passivity control," *IEEE Trans. Control Syst. Technol.*, vol. 25, no. 3, pp. 991–1006, May 2017.

[11] S. Mehrdad et al., "Review of advanced medical telerobots," *Appl. Sci.*, vol. 11, no. 1, 2020, Art. no. 209.

[12] V. Chawda and M. K. O'Malley, "Position synchronization in bilateral teleoperation under time-varying communication delays," *IEEE/ASME Trans. Mechatron.*, vol. 20, no. 1, pp. 245–253, Feb. 2015.

[13] N. Feizi, R. V. Patel, M. R. Kermani, and S. F. Atashzar, "Adaptive wave reconstruction through regulated-BMFLC for transparency-enhanced telerobotics over delayed networks," *IEEE Trans. Robot.*, vol. 38, no. 5, pp. 2928–2942, Oct. 2022.

[14] P. Paik, S. Thudi, and S. F. Atashzar, "Power-based velocity-domain variable structure passivity signature control for physical human-(tele) robot interaction," *IEEE Trans. Robot.*, vol. 39, no. 1, pp. 386–398, Feb. 2023.

[15] F. Porcini, M. Solazzi, and A. Frisoli, "Optimal joint TDPA formulation for kinematically redundant robot manipulators," in *Proc. IEEE/RSJ Int. Conf. Intell. Robots Syst.*, 2022, pp. 7742–7749.

[16] Y. Shen, J. Ma, B. Dobkin, and J. Rosen, "Asymmetric dual arm approach for post stroke recovery of motor functions utilizing the exo-ul8 exoskeleton system: A pilot study," in *Proc. IEEE 40th Annu. Int. Conf. Eng. Med. Biol. Soc.*, 2018, pp. 1701–1707.

[17] N. F. Rad and R. Nagamune, "Adaptive energy reference time domain passivity control of teleoperation systems in the presence of time delay," in *Proc. IEEE Int. Symp. Adv. Control Ind. Processes*, 2022, pp. 307–312.

[18] H. Singh et al., "Preserving the physical coupling in teleoperation despite time delay through observer-based gradient control," *IFAC-PapersOnLine*, vol. 52, no. 18, pp. 25–30, 2019.

[19] A. Coelho, H. Singh, T. Muskardin, R. Balachandran, and K. Kondak, "Smoother position-drift compensation for time domain passivity approach based teleoperation," in *Proc. IEEE/RSJ Int. Conf. Intell. Robots Syst.*, 2018, pp. 5525–5532.

[20] M. Laghi et al., "Unifying bilateral teleoperation and tele-impedance for enhanced user experience," *Int. J. Robot. Res.*, vol. 39, no. 4, pp. 514–539, 2020.

[21] L. M. Doornebosch, D. A. Abbink, and L. Peternel, "Analysis of coupling effect in human-commanded stiffness during bilateral tele-impedance," *IEEE Trans. Robot.*, vol. 37, no. 4, pp. 1282–1297, Aug. 2021.

[22] Y. Yang, D. Constantinescu, and Y. Shi, "Passive multiuser teleoperation of a multirobot system with connectivity-preserving containment," *IEEE Trans. Robot.*, vol. 38, no. 1, pp. 209–228, Feb. 2022.

[23] J.-H. Ryu, D.-S. Kwon, and B. Hannaford, "Stability guaranteed control: Time domain passivity approach," *IEEE Trans. Control Syst. Technol.*, vol. 12, no. 6, pp. 860–868, Nov. 2004.

[24] S. P. Buerger and N. Hogan, "Complementary stability and loop shaping for improved human–robot interaction," *IEEE Trans. Robot.*, vol. 23, no. 2, pp. 232–244, Apr. 2007.

[25] E. Spyrakos-Papastavridis, P. R. N. Childs, and J. S. Dai, "Passivity preservation for variable impedance control of compliant robots," *IEEE/ASME Trans. Mechatronics*, vol. 25, no. 5, pp. 2342–2353, Oct. 2020.

[26] B. Hannaford and J.-H. Ryu, "Time-domain passivity control of haptic interfaces," *IEEE Trans. Robot. Automat.*, vol. 18, no. 1, pp. 1–10, Feb. 2002.

[27] M. Panzirsch, M. Sierotowicz, R. Prakash, H. Singh, and C. Ott, "Deflection-domain passivity control of variable stiffnesses based on potential energy reference," *IEEE Robot. Automat. Lett.*, vol. 7, no. 2, pp. 4440–4447, Apr. 2022.

[28] D. Shi et al., "A review on lower limb rehabilitation exoskeleton robots," *Chin. J. Mech. Eng.*, vol. 32, no. 1, pp. 1–11, 2019.

[29] L. S. Uiterkamp, F. Porcini, G. Englebienne, A. Frisoli, and D. Dresscher, "EMG-based feedback modulation for increased transparency in teleoperation," in *Proc. IEEE/RSJ Int. Conf. Intell. Robots Syst.*, 2022, pp. 599–604.

[30] S. F. Atashzar, H.-Y. Huang, F. D. Duca, E. Burdet, and D. Farina, "Energetic passivity decoding of human hip joint for physical human-robot interaction," *IEEE Robot. Automat. Lett.*, vol. 5, no. 4, pp. 5953–5960, Oct. 2020.

[31] F. H. Netter, *Atlas of Human Anatomy E-Book*, 7th ed.Philadelphia, PA, USA:Elsevier, 2017.

[32] G. Herrnstadt and C. Menon, "Voluntary-driven elbow orthosis with speed-controlled tremor suppression," *Front. Bioeng. Biotechnol.*, vol. 4, 2016, Art. no. 29.

[33] H. Yang, J. Wan, Y. Jin, X. Yu, and Y. Fang, "EEG and EMG driven post-stroke rehabilitation: A review," *IEEE Sensors J.*, vol. 22, no. 24, pp. 23649–23660, Dec. 2022.

[34] H. K. Khalil and J. Grizzle, *Nonlinear Systems*, vol. 3. Hoboken, NJ, USA: Prentice Hall, 2002.

[35] J. Verma and A.-S. G. Abdel-Salam, *Testing Statistical Assumptions in Research*. Hoboken, NJ, USA: Wiley, 2019.